von Hippel, P. H., Kowalczykowski, S. C., Lonberg, N., Newport, J. W., Paul, L. S., Stormo, G. D., & Gold, L. (1982) *J. Mol. Biol. 162*, 795–818.
Weber, K., & Konigsberg, W. (1975) in *RNA Phages* (Zinder, N., Ed.) pp 51–84, Cold Spring Harbor Laboratory, Cold Spring Harbor, NY.
Witherell, G. W., & Uhlenbeck, O. C. (1989) *Biochemistry 28*, 71–76.
Yanisch-Perron, C., Vieira, J., & Messing, J. (1985) *Gene 33*, 103–119.

Structural Features of the Protoporphyrin–Apomyoglobin Complex: A Proton NMR Spectroscopy Study†

Juliette T. J. Lecomte* and Melanie J. Cocco
Department of Chemistry, 152 Davey Laboratory, The Pennsylvania State University, University Park, Pennsylvania 16802
Received July 23, 1990; Revised Manuscript Received August 30, 1990

ABSTRACT: The structural properties of the complex formed by apomyoglobin and protoporphyrin IX (des-iron myoglobin) were studied to probe the influence of iron-to-histidine coordination on the native myoglobin fold and the heme binding site geometry. Standard two-dimensional proton nuclear magnetic resonance spectroscopy methods were applied to identify porphyrin and protein signals. A pronounced spectral resemblance between carbonmonoxymyoglobin and des-iron myoglobin was noticed that could be exploited to assign a number of resonances by nuclear Overhauser spectroscopy. Protoporphyrin IX was determined to bind in the same orientation as the heme. Most residues in contact with the prosthetic group were found in the holomyoglobin conformation. Several tertiary structure features were also characterized near the protein termini. It was concluded that the protoporphyrin–apomyoglobin interactions are capable of organizing the binding site and the unfolded region of the apoprotein into the native holoprotein structure.

Myoglobin (Mb)[1] is a *b* heme protein naturally used for oxygen storage. Its single prosthetic group resides in a tight crevice lined with hydrophobic residues (Takano, 1977a,b). The interactions that fasten the heme to the protein matrix fall in three classes. There are van der Waals contacts between the hydrophobic side chains and the heme π system, coordination of the central iron atom to the proximal histidine, and electrostatic interactions between the heme propionate side chains and residues bordering the cavity. Sperm whale apomyoglobin studies have demonstrated that the heme group not only plays a functional role but also allows Mb to adopt and maintain the correct native fold: disruption of the heme–protein interactions results in a structure that is ca. 25% less helical (Harrison & Blout, 1965) and ca. 23 kJ less stable (Griko et al., 1988a,b) than the holoprotein.

The relative importance of the various heme–protein interactions in forcing the unwound elements into the native holoMb conformation has been a matter of interest for many years. In 1967, Breslow and co-workers investigated the structural role of the Fe–His bond by using an artificial Mb containing protoporphyrin IX (PrIX) as prosthetic group (Breslow et al., 1967). This protein differs in composition from native Mb by the absence of the iron and is therefore referred to as des-Fe Mb. It was then shown that coordination of the proximal His stabilizes the holoprotein but does not affect the extent of secondary structure measured by CD spectroscopy. Most tertiary interactions also appear to be formed in des-Fe Mb, since it behaves as the holoprotein with respect to pH titration and bromoacetate modification of histidine side chains (Breslow & Koehler, 1965). However, fluorescence depolarization (Albani & Alpert, 1986) and immunoassay experiments (Atassi, 1967) reflect subtle dynamic and structural differences between the two complexes.

The novel ability to engineer mutations in myoglobin and the interest in the structure–function relationship manifested by these altered proteins (Braunstein et al., 1988; Springer et al., 1989; Varadarajan et al., 1989a,b) prompted us to examine the interactions holding PrIX in the heme cavity and determine the position of binding-site residues in the absence of coordination to a central ion. We chose ^{1}H NMR spectroscopy as the most promising method for analyzing the structural details of this modified protein. For a complete description of the structural role of the prosthetic group, complementary information must be gathered on the apoprotein. A parallel study of apomyoglobin was undertaken, whose results are presented in the companion paper (Cocco & Lecomte, 1990).

Materials and Methods

Apomyoglobin. Apomyoglobin was prepared from horse skeletal myoglobin (Sigma Type I) or sperm whale myoglobin (Sigma) by using the methyl ethyl ketone method introduced by Teale (1955). Residual heme content was lower than 1%

† Acknowledgment is made to the donors of the Petroleum Research Fund, administered by the American Chemical Society, for support of this work.
* To whom correspondence should be addressed.

[1] Abbreviations: apoMb, apomyoglobin; CD, circular dichroism; des-Fe Mb, des-iron myoglobin; COSY, correlated spectroscopy; 2D, two-dimensional; DQF-COSY, double-quantum-filtered COSY; Eq, equine; holoMb, holomyoglobin; Mb, myoglobin; MbCN, metcyanomyoglobin; MbCO, carbonmonoxymyoglobin; met, ferric form of myoglobin; NMR, nuclear magnetic resonance; NOE, nuclear Overhauser effect; NOESY, two-dimensional proton nuclear Overhauser spectroscopy; PrIX, protoporphyrin IX; SW, sperm whale; TOCSY, total correlation spectroscopy; 2Q, two-quantum.

0006-2960/90/0429-11057$02.50/0

as evaluated by the ratio of absorbances at 280 and 410 nm. ApoMb was lyophilized for long-term storage.

Des-Iron Myoglobin. Protoporphyrin IX was purchased from Porphyrin Products. For reconstitution with apoMb, PrIX was dissolved in 0.01 M NaO^2H or NaOH and the residual solid removed by centrifugation. In the absence of direct light, 1.5–2 equiv of the dissolved PrIX was added to the apoprotein in ^2H_2O or ^1H_2O. During this process, the pH was maintained below 8. Excess PrIX was removed by lowering the pH to 5.8 and filtering through an Amicon Centricon-10 microconcentrator (YM10 membrane). Des-Fe Mb was identified by its typical absorption at 408 nm (Atassi, 1967; Breslow et al., 1967). PrIX is an efficient photosensitizer, and exposure of des-Fe Mb to light in the presence of oxygen results in the photooxidation of histidine residues (Breslow et al., 1967; Mauk & Girotti, 1973). To insure that the material used in the NMR experiments was not photooxidized, all precautions were taken to keep the samples in darkness and an additional control was performed as follows. A sample of des-Fe Mb was prepared and kept in the dark for a period of time comparable to that of an average NMR data collection. The porphyrin was extracted from the sample, hemin was added to the apoprotein, and the mixture was left to equilibrate for 24 h. Excess KCN was then added to produce the low-spin metcyano complex of the reconstituted holoprotein, and the proton spectrum of the complex was recorded in 90% ^1H_2O/10% ^2H_2O at pH 8.03, without solvent suppression. The characteristic ring NH signals from His 93 (proximal), His 64 (distal), and His 97 (Cutnell et al., 1981) were detected with appropriate intensities: no evidence of photooxidation was found. Protected from exposure to light, des-Fe Mb remains stable in solution for about 2 weeks as judged from the NMR spectra. Lyophilization destroys the complex. Des-iron myoglobin appears to be a homogeneous complex as soon as an NMR spectrum can be recorded (3 min after reconstitution and without the purification and concentration steps described above).

Carbonmonoxymyoglobin. Horse MbCO was prepared as reported by others (Mabbutt & Wright, 1985), except that excess dithionite was removed by ultrafiltration through an Amicon Centricon-10 microconcentrator using CO purged ^2H_2O or ^1H_2O. The MbCO samples were checked for the presence of autoxidation product by recording periodically an NMR spectrum over a frequency window covering the metaquo Mb signals (>140 ppm).

NMR Samples. NMR samples were 2–3 mM in protein and kept at 4 °C when not in use. The pH of all samples was adjusted to 5.7 with a Beckman Φ71 pH meter equipped with an Ingold combination microelectrode. For ^2H_2O samples, exchange was accomplished in a Centricon-10 microconcentrator, using 10 volumes of 99.96% ^2H_2O. The pH of ^2H_2O samples was not corrected for isotope effect and is reported as pH*. All NMR experiments were run at 298 K.

NMR Measurements. Proton NMR spectra were acquired at 500 MHz on a Bruker AM-500 spectrometer equipped with an Aspect 3000 computer and digital phase-shifting hardware. Transmitter and decoupler frequencies were set equal to that of the water line and were derived from the same source. The 90° transmitter pulse was on the order of 7 μs. Suppression of the water resonance was achieved through saturation during the relaxation delay and the mixing time. All two-dimensional spectra were recorded in the phase-sensitive mode as implemented through the time-proportional increment method (Drobny et al., 1979; Marion & Wüthrich, 1983). DQF-COSY spectra (Rance et al., 1983) were collected over 2048 complex points with 64 transients per each of the 512 t_1 increments. The spectral width was 8928 Hz in the ω_1 and ω_2 dimensions. Two-quantum spectra (Braunschweiler et al., 1983; Rance & Wright, 1986) were recorded by using the standard procedure with total mixing times ranging from 22 to 80 ms. For these experiments, the spectral width was 6024 Hz in the ω_2 dimension and the t_1 increment was such as to yield a 11 904-Hz width in the ω_1 dimension. Ninety-six transients were collected per each of the 512 t_1 values. TOCSY spectra (Braunschweiler & Ernst, 1983) were recorded over a 12 500-Hz width (4096 complex points) to improve the baseline and with a 75-ms mixing time. Locking was achieved with an MLEV-17 sequence (Bax & Davis, 1985), producing an effective field of 6.6 kHz. Hahn-echo NOESY experiments (Kumar et al., 1980; Bodenhausen et al., 1984; Davis, 1989) were collected over the same width with mixing times varying between 80 and 160 ms. No evidence of spin diffusion was noted up to 150 ms. All NOEs reported here at long mixing times were also observed at shorter τ_m values unless otherwise specified. Both the TOCSY and NOESY experiments were recorded with the zero-order phase correction set to zero by adjusting the reference phase as needed. Ninety-six transients were collected per each of the 512 t_1 increments.

Data were processed on a microVax II computer with the program FTNMR (Hare Research, Inc., Woodinville, WA). The raw data matrix was transformed with zero-filling in the t_1 dimension to obtain a (4096 or 2048 × 1024)-complex-point matrix. When necessary, a polynomial baseline correction (zero or third order) was applied to the ω_2 domain before transforming in the t_1 domain and/or in the ω_1 domain after the second transform. Data presented in the figures were filtered with sine-bell multiplication (shift of 22.5° in the t_2 domain reduced to ca. 1600 nonzero data points and 40° in the t_1 domain). The free induction decay corresponding to the first t_1 value of the NOESY and TOCSY data set was divided by 2 to suppress ridges in the ω_1 dimension (Otting et al., 1986). All spectra were processed and plotted in the phase-sensitive mode. Chemical shifts are referred to the water line at 4.76 ppm.

RESULTS

Assignment Strategy. Upon reconstitution of apomyoglobin with PrIX, the stable des-Fe Mb compound is formed. Des-Fe Mb yields a ^1H NMR spectrum that spans a large chemical shift range (La Mar et al., 1989) and is reasonably well resolved for a 17-kDa protein. The dispersion is a manifestation of the ring current generated by the bound PrIX and of the secondary and tertiary structure recovery. In fact, the overall appearance of the des-Fe Mb spectrum resembles that of the diamagnetic MbCO spectrum. The latter complex provides a convenient reference for spectral assignments.

Our study focuses on myoglobin extracted from horse skeletal muscle. Unfortunately, little NMR information is available for the intended reference, horse MbCO. Sperm whale MbCO, in contrast, has been the subject of extensive NMR investigation (Mabbutt & Wright, 1985; Dalvit & Wright, 1987). Because horse and sperm whale Mbs have high sequence homology (Dayhoff, 1976) and for our purposes, practically identical structures (Evans & Brayer, 1988), the assignment process was much aided by the extant sperm whale data. For the large majority of assigned residues, it is found that the line positions in horse MbCO are within less than 0.2 ppm of those in sperm whale MbCO. In what follows, we concentrate on the des-Fe complex and limit our discussion of the horse MbCO data to the residues unique to this protein.

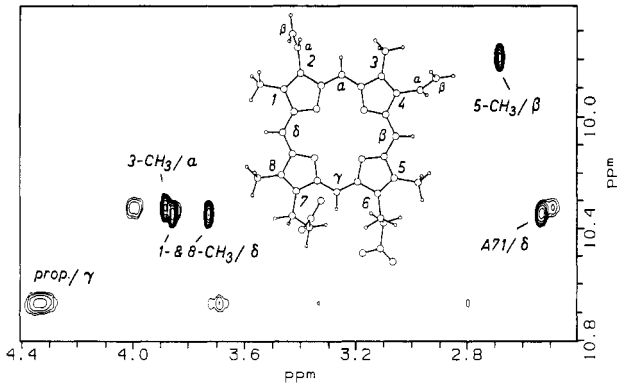

FIGURE 1: Region of a phase-sensitive NOESY spectrum (τ_m = 100 ms) recorded on horse des-Fe Mb in 90% ^1H_2O/10% ^2H_2O at pH 5.7 and 298 K. The stronger cross peaks are due to dipolar contact between porphyrin meso protons and porphyrin methyl groups. The NOE connecting a broad signal at 4.34 ppm to the γ-*meso*-H (labeled prop.) arises from a 6-propionate proton. Also marked is an NOE between the δ-*meso*-H and Ala 71 $C^\beta H_3$. The inset is placed in a region of the spectrum where no NOEs of comparable intensity are observed; it illustrates the skeleton of the porphyrin ring as found in sperm whale MbCO (Hanson & Schoenborn, 1981) and the nomenclature used in this work.

The procedure was repeated for the horse des-Fe complex, and to ensure consistency, several experiments were performed on sperm whale des-Fe Mb as well.

The assignment strategy was modeled directly after that applied to sperm whale MbCO. In a first phase, the results of various two-dimensional phase-sensitive correlated experiments (DQF-COSY, 2Q, and TOCSY) were combined to delineate scalar connectivities and identify spin systems. We focused on hydrophobic and histidine residues, as they are known to line the binding site and are likely to participate in stable cores both in des-Fe Mb and in the apoprotein.

The second phase is the assignment of the identified spin systems to specific side chains. This was achieved by perusing the spatial relationship uncovered in the NOESY experiments and comparing to those predicted by the neutron diffraction structure of MbCO (Hanson & Schoenborn, 1981). The simplest route consists of (i) assignment of the porphyrin resonances, (ii) assignment of the signals arising from residues in contact with porphyrin substituents, and (iii) assignment of the signals arising from residues located farther from the porphyrin. Comparison of data among the four proteins often resolved ambiguities.

(*i*) *Porphyrin Resonances.* A schematic porphyrin ring and the nomenclature used in this work are presented within Figure 1. In the proton spectrum of des-Fe Mb, as in that of MbCO, the two porphyrin vinyl side chains are readily identified by a nonproteinic DQF-COSY pattern. They give rise to two α-H resonances at ca. 8.6 ppm and two pairs of β resonances centered at 6.75 and 5.92 ppm. When resolved, β_{cis} and β_{trans} protons are discriminated by the magnitude of the coupling constant to the α proton. The meso protons resonate downfield from all nonexchangeable proton peaks, between 9.8 and 10.7 ppm. Figure 1 contains a portion of a phase-sensitive NOESY spectrum of horse des-Fe Mb recorded in 90% ^1H_2O/10% ^2H_2O that includes the *meso*-H/PrIX-CH_3 cross peaks. PrIX methyl groups occur as four sharp singlets between 2.6 and 4.0 ppm. The δ-*meso*-H is the only one in dipolar contact with two porphyrin methyl groups (1- and 8-CH_3) and is assigned at 10.36 ppm. The 1-CH_3 is distinguished from the 8-CH_3 by its NOEs to one of the vinyl groups. From the δ-*meso*-H, the following connectivities are therefore traced around the ring: 8-CH_3 ← δ-*meso*-H → 1-CH_3 → 2-vinyl → α-*meso*-H → 3-CH_3 → 4-vinyl → β-*meso*-H → 5-CH_3.

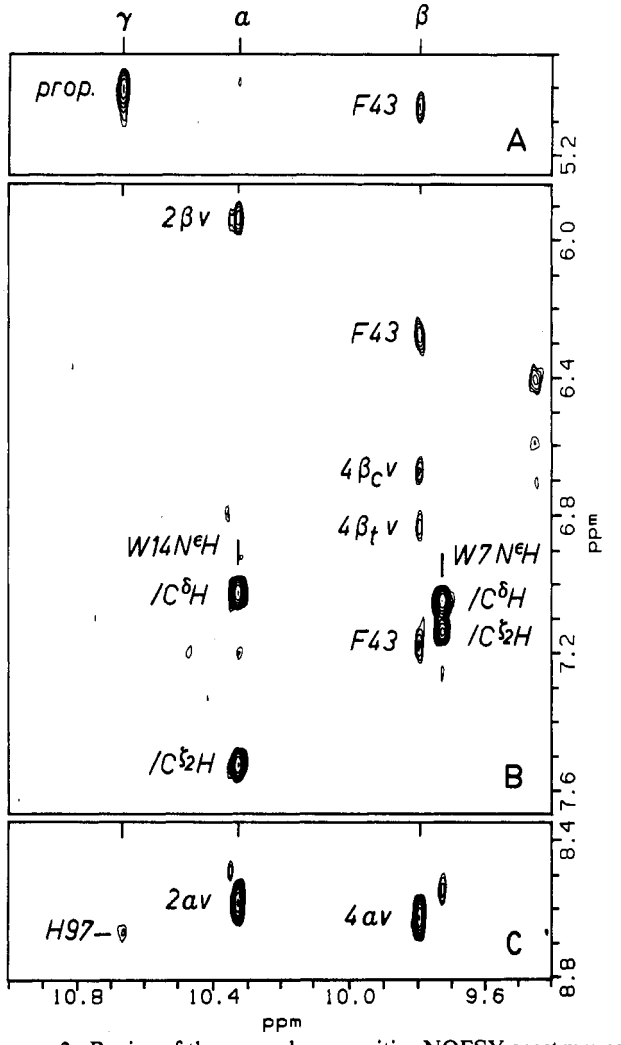

FIGURE 2: Region of the same phase-sensitive NOESY spectrum as shown in Figure 1. The marks γ, α, and β indicate the chemical shift (δ_2) of three porphyrin meso protons. Panels A, B, and C correspond to different sections in the δ_1 dimension. Note that all ring protons of Phe 43 are in contact with the β-*meso*-H. Also in this spectrum are the cross peaks identifying the $C^\delta H$ and $C^{\zeta 2}H$ of Trp 7 and Trp 14. For both vinyl side chains, strong NOEs are observed from the α proton to the nearest meso proton. NOEs from the vinyl β protons to the same meso proton are weaker. A weak but reproducible cross peak is observed between the γ-*meso*-H and the $C^\epsilon H$ of His 97. The NOE connecting a broad signal at 5.02 ppm to the γ-*meso*-H (labeled prop.) arises from a 7-propionate proton.

The γ-*meso*-proton, between the two propionate side chains, resonates at 10.67 ppm and presents several broad cross peaks between 5.1 and 2.5 ppm. The two stronger ones are seen in Figure 1 (at 4.31 ppm) and in Figure 2A (at 5.02 ppm), which presents another region of the NOESY spectrum of Figure 1. The proton at 4.31 ppm exhibits a scalar coupling cross peak at 3.71 ppm; both protons are in dipolar contact with the γ-*meso*-H and also the 5-CH_3 group. They are attributed to the 6-propionate side chain. Similar arguments apply to the peak at 5.02 ppm. It is coupled to a signal at 4.30 ppm and both protons are close to the γ-*meso*-H and the 8-CH_3 group. Assignment to the 7-propionate side chain follows. Additional DQF-COSY, TOCSY, and NOESY information was used to assign four remaining protons near the γ-*meso*-H to one or the other propionate side chain. Chemical shifts for PrIX in horse and sperm whale des-Fe Mb are listed in Table I.

The intra-prosthetic-group NOEs and chemical shifts observed in des-Fe Mb are directly comparable to those in MbCO. For example, the β-*meso*-H and 5-CH_3 nuclei experience more shielding than the other meso and methyl

Table I: Protoporphyrin IX Assignments in Horse and Sperm Whale Des-Iron Myoglobin[a]

	des-Fe EqMb	des-Fe SWMb	EqMbCO[b]	SWMbCO[c]
meso protons				
α	10.32	10.36	9.89	9.92
β	9.79	9.78	9.37	9.34
γ	10.67	10.67	10.07	10.15
δ	10.35	10.35	9.84	9.86
vinyl protons				
2-α	8.58	8.60	8.42	8.43
2-β_{trans}	5.93	5.99	5.69	5.73
2-β_{cis}	5.93	5.93	5.69	5.69
4-α	8.62	8.58	8.67	8.62
4-β_{trans}	6.83	6.83	6.61	6.61
4-β_{cis}	6.67	6.67	6.27	6.29
methyl protons				
1	3.86	3.83	3.64	3.63
3	3.88	3.88	3.78	3.79
5	2.68	2.77	2.46	2.53
8	3.73	3.73	3.56	3.59
propionate protons				
6-α	4.34[d]	4.31[d]	nd	na
6-α'	3.71	3.71	nd	na
6-$\beta(\beta')$	2.79	2.86	nd	na
6-$\beta'(\beta)$	2.59	2.66	nd	na
7-$\alpha(\alpha')$	3.35	3.34	nd	na
7-$\alpha'(\alpha)$	3.07	3.06	nd	na
7-β	4.33	4.30	nd	na
7-β'	5.02[d]	5.02[d]	nd	na

[a] Chemical shifts in parts per million with respect to residual $^1H^2HO$ at 4.76 ppm, determined at pH* 5.7, 298 K. The labeling scheme is presented in Figure 1. MbCO values are included for comparison. [d] Determined at pH* 5.7, 298 K (this work); nd, not determined. [c] Determined at pH* 7.0, 308 K; from Mabbutt and Wright (1985); na, not available. [d] Distinction between α and β protons was achieved by comparing the size of the NOEs to the γ-*meso*-H and using the neutron diffraction structure of Hanson and Schoenborn (1981) to evaluate internuclear distances; α' and β' refer to the second α or β proton as listed in the Brookhaven Protein Data Bank coordinates 1mb5.

protons, the γ-*meso*-proton resonates systematically most downfield, and the 2-vinyl β protons practically overlap. The orientation of the vinyl groups can be deduced from the NOEs shown in Figure 2B. Both the 2- and 4-vinyl α protons have strong NOEs to the nearest meso proton, whereas the β_{trans} protons exhibit NOEs to the nearest PrIX methyl group and weak NOEs to the nearest meso proton. The pattern is consistent with vinyl side chains in the cis conformation. Porphyrin and iron–porphyrin therefore seem to bind in the same fashion to the protein matrix.

(*ii*) *Protein Resonances.* The porphyrin protons provide spatial probes from which the environment of the prosthetic group can be explored. Table II contains reported sperm whale MbCO assignments (Dalvit & Wright, 1987), assignments for sperm whale des-Fe Mb, and corresponding chemical shift values obtained for horse MbCO and des-Fe Mb. A list of key NOE connectivities is provided in Table III.

Phe 43. DQF-COSY and TOCSY spectra of des-Fe Mb show a well-resolved phenylalanine pattern between 5.0 and 7.3 ppm. Figure 2 illustrates the NOEs observed from this ring to the 10.7–9.8 ppm region of the spectrum. Dipolar connectivities to the β-*meso*-H place the side chain in contact with the porphyrin. Neutron diffraction (Hanson & Schoenborn, 1981) and NMR data on MbCO point to Phe 43, a residue located on the distal side of the binding site. Contacts are also seen to the 5-CH_3 group, in agreement with a conserved orientation of the ring with respect to the porphyrin.

Val 67, Val 68, and Ala 71. In the aliphatic region, the most upfield-shifted signal resonates at ca. −3.7 ppm and has DQF-COSY and TOCSY patterns indicating a valine methyl

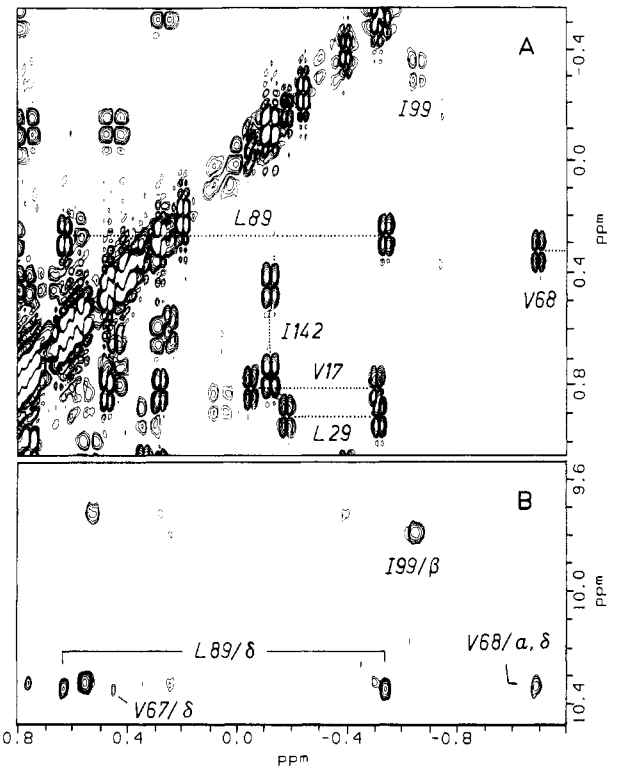

FIGURE 3: Combined DQF-COSY–NOESY spectra of a sample of horse des-Fe Mb in 90% ^1H_2O/10% ^2H_2O at pH 5.7 and 298 K. (A) The DQF-COSY spectrum illustrates J connectivities observed for several aliphatic residues. Positive and negative levels are plotted without distinction. The cross peak at $\delta_2 = -1.05$ ppm and $\delta_1 = 0.36$ ppm connects the $C^{\gamma 1}H_3$ of Val 68 to its $C^{\beta}H$. The other methyl group resonates at −3.64 ppm. At $\delta_2 = -0.62$ ppm and $\delta_1 = -0.30$ ppm, a broad cross peak illustrates the connectivity between the $C^{\gamma 1}$ protons of Ile 99. Dotted lines connect $C^{\delta 1}H_3$–$C^{\gamma}H$ and $C^{\delta 2}H_3$–$C^{\gamma}H$ cross peaks (Leu 89 and Leu 29) as well as $C^{\gamma 1}H_3$–$C^{\beta}H$ and $C^{\gamma 2}H_3$–$C^{\beta}H$ cross peaks (Val 17). Also marked are the $C^{\delta}H_3$–$C^{\gamma 1}H$ cross peaks of Ile 142. (B) The phase-sensitive NOESY spectrum (conditions as in Figure 1) shows the proximity of Ile 99 to the β-*meso*-H, of Leu 89 to the δ-*meso*-H, and of Val 68 to the α- and δ-*meso*-H. A weaker NOE from Val 67 to the δ-*meso*-H is also indicated.

group with a companion methyl at −1.05 ppm. A strong NOE from −3.7 ppm to the δ-*meso*-H, as well as NOEs from −1.05 ppm to the α-*meso*-H, δ-*meso*-H, the 1-CH_3, and the 2-vinyl side chain, manifest proximity to the porphyrin ring and assign the residue as Val 68, a distal side chain packed against the prosthetic group. Val 68 is preceded by Val 67 in horse Mb and by Thr 67 in sperm whale Mb. This replacement is the only one occurring inside the binding site; X-ray diffraction data place Val 67 and Thr 67 in the same conformation (Evans & Brayer, 1988). Val 67 is identified through its J-coupling pattern and assigned by NOEs to the 8-CH_3 group, the γ-*meso*-H, and Val 68. Corresponding contacts are observed for Thr 67 in the sperm whale des-Fe Mb spectrum. NOEs from the 1- and 8-CH_3 groups and the δ-*meso*-H to an alanine $C^{\beta}H_3$ group at 2.55 ppm assign Ala 71. The latter effect is included in Figure 1. At mixing times longer than 100 ms, NOEs between Ala 71 and Val 68 are detected in both horse and sperm whale des-Fe Mb.

Leu 89, His 97, Ile 99, Leu 104, and Phe 138. Figure 3A provides a section of the DQF-COSY spectrum of horse des-Fe Mb. The $C^{\gamma}H/C^{\delta}H_3$ cross peaks of a leucine spin system are found at $\delta_2 = -0.52$ ppm and $\delta_2 = 0.65$ ppm. Figure 3B contains NOE data corresponding to this residue: both methyl groups are close to the δ-*meso*-H. One of them is near Ala 71, a constraint that dictates assignment to Leu 89. Leu 89 is in close proximity to an aromatic ring with resonances

Table II: Sequence-Specific Proton Resonance Assignments for Horse and Sperm Whale Des-Iron Myoglobin[a]

residue	proton[b]	des-Fe EqMb	des-Fe SWMb	EqMbCO[c]	SWMbCO[d]	residue	proton[b]	des-Fe EqMb	des-Fe SWMb	EqMbCO[c]	SWMbCO[d]
Leu 2	$C^{\beta}H$	0.12	nd	nd	na	Leu 69	$C^{\gamma}H$	1.71	1.69	1.75	na
	$C^{\gamma}H$	1.13	1.13	1.16	na		$C^{\delta 1}H_3$	0.59	0.58	0.77	na
	$C^{\delta 1}H_3$	0.31	0.38	0.28	na		$C^{\delta 2}H_3$	0.76	0.72	0.60	na
	$C^{\delta 2}H_3$	−0.37	−0.37	−0.41	na	Ala 71	$C^{\alpha}H$	4.64	4.68	4.59	4.63
Trp 7	$C^{\delta}H$	7.05	6.95	7.04	6.97		$C^{\beta}H_3$	2.55	2.54	2.43	2.41
	$N^{\epsilon}H$	9.73	9.73	9.74	9.74	Leu 89	$C^{\alpha}H$	3.59	3.60	nd	3.74
	$C^{\zeta 2}H$	7.15	7.16	7.13	7.15		$C^{\beta}H$	1.42	1.42	nd	1.48
	$C^{\eta}H$	7.29	7.29	7.28	7.27		$C^{\beta'}H$	nd	nd	nd	1.18
	$C^{\zeta 3}H$	7.06	7.07	7.07	7.08		$C^{\gamma}H$	0.30	0.24	0.63	0.63
	$C^{\epsilon 3}H$	7.47	7.45	7.46	7.45		$C^{\delta 1}H_3$	−0.52	−0.72	0.29	0.31
Trp 14	$C^{\delta}H$	7.04	6.99	7.04	7.04		$C^{\delta 2}H_3$	0.65	0.65	0.42	0.44
	$N^{\epsilon}H$	10.25	10.31	10.30	10.29	Ala 94	$C^{\alpha}H$	2.81	3.03	2.90	3.10
	$C^{\zeta 2}H$	7.52	7.49	7.59	7.52		$C^{\beta}H_3$	0.77	0.85	0.46	0.31
	$C^{\eta}H$	6.94	6.92	6.97	6.92	His 97	$C^{\epsilon}H$	8.67	8.61	8.30	8.54
	$C^{\zeta 3}H$	6.72	6.71	6.70	6.69	Ile 99	$C^{\alpha}H$	3.91	3.98	nd	4.29[e]
	$C^{\epsilon 3}H$	7.13	7.13	7.15	7.14		$C^{\beta}H$	0.62	0.56	nd	1.13[e]
Val 17	$C^{\alpha}H$	1.69	1.50	1.74	1.58		$C^{\gamma 1}H$	−0.30	−0.44	nd	0.85[e]
	$C^{\beta}H$	0.85	0.83	0.88	0.86		$C^{\gamma 1'}H$	−0.62	−0.32	nd	−0.28[e]
	$C^{\gamma 1}H_3$	−0.47	−0.47	−0.47	−0.45		$C^{\gamma 2}H_3$	0.27	0.12	nd	1.36[e]
	$C^{\gamma 2}H_3$	−0.01	−0.13	−0.04	−0.11		$C^{\delta}H_3$	−2.09	−2.70	nd	1.47[e]
His 24	$C^{\delta}H$	6.25	6.28	6.26	6.31	Tyr 103	$C^{\delta/\epsilon}H$	7.18	7.20	7.21	7.23
	$C^{\epsilon}H$	7.97	7.85	7.99	7.94		$C^{\epsilon/\delta}H$	7.30	7.38	7.30	7.31
Leu 29	$C^{\beta}H$	0.34	0.39	0.11	0.19	Leu 104	$C^{\alpha}H$	5.00	5.02	nd	na
	$C^{\gamma}H$	0.95	1.01	0.84	0.86		$C^{\beta}H$	2.45	2.38	nd	na
	$C^{\delta 1}H_3$	−0.15	−0.15	−0.25	−0.26		$C^{\beta'}H$	2.77	2.82	nd	na
	$C^{\delta 2}H_3$	−0.48	−0.41	−0.71	−0.67		$C^{\gamma}H$	1.78	1.83	nd	na
Phe 33	$C^{\delta}H$	7.08	7.14	6.93	7.01		$C^{\delta 1}H_3$	1.11	1.12	nd	na
	$C^{\epsilon}H$	6.60	6.67	6.37	6.45		$C^{\delta 2}H_3$	0.62	0.63	nd	na
	$C^{\zeta}H$	5.62	5.77	5.06	5.22	Phe 106	$C^{\delta}H$	6.92	6.84	6.90	6.81
His 36	$C^{\delta}H$	7.18	7.18	7.17	7.12		$C^{\epsilon,\zeta}H$	7.43	7.42	7.44	7.44
	$C^{\epsilon}H$	8.06	8.17	8.06	8.15	Leu 115	$C^{\gamma}H$	1.69	1.75	1.70	na
Leu 40	$C^{\gamma}H$	1.24	1.28	1.17	na		$C^{\delta 1}H_3$	0.66	0.68	0.67	na
	$C^{\delta 1}H_3$	0.43	0.34	0.32	na		$C^{\delta 2}H_3$	0.48	0.51	0.47	na
	$C^{\delta 2}H_3$	0.23	0.28	0.11	na	His 119	$C^{\delta}H$	6.85	6.77	6.97	6.92
Phe 43	$C^{\delta}H$	7.20	7.15	7.21	7.29		$C^{\epsilon}H$	8.51	8.41	8.57	8.61
	$C^{\epsilon}H$	6.27	6.22	6.10	6.08	Phe 123	$C^{\delta}H$	7.08	7.11	7.04	7.10
	$C^{\zeta}H$	5.09	5.16	4.67	4.72		$C^{\epsilon}H$	7.30	7.38	7.25	7.32
Phe 46	$C^{\alpha}H$	5.10	5.12	5.05	na		$C^{\zeta}H$	7.18	7.21	7.16	7.19
	$C^{\delta}H$	6.63	6.68	6.67	6.74	Met 131	$C^{\epsilon}H_3$	2.25	2.25	2.25	2.25
	$C^{\epsilon}H$	6.50	6.49	6.51	6.52	Phe 138	$C^{\delta}H$	7.14	7.15	7.07	7.08
	$C^{\zeta}H$	6.39	6.29	6.63	6.56		$C^{\epsilon}H$	7.21	7.18	7.11	7.15
His 48	$C^{\delta}H$	7.12	7.12	7.12	7.17		$C^{\zeta}H$	7.09	7.06	6.98	7.00
	$C^{\epsilon}H$	8.21	8.20	8.25	8.32	Ile 142	$C^{\alpha}H$	3.24	nd	nd	3.34
Met 55	$C^{\epsilon}H_3$	1.71	1.78	1.70	1.76		$C^{\beta}H$	1.29	1.20	1.28	1.28
His 64	$C^{\delta}H$	4.96	4.95	4.83	4.97		$C^{\gamma 1/\gamma 1'}H$	0.47	0.54	0.43	0.55
Val 67	$C^{\alpha}H$	3.38		nd			$C^{\gamma 1'/\gamma 1}H$	0.80	0.73	0.74	0.77
	$C^{\beta}H$	1.34		1.88			$C^{\gamma 2}H_3$	−0.22	−0.18	−0.19	−0.03
	$C^{\gamma 1}H_3$	0.47		1.07			$C^{\delta}H_3$	−0.09	−0.06	−0.21	−0.10
	$C^{\gamma 2}H_3$	0.89		0.65		Tyr 146	$C^{\epsilon}H$	6.44	6.44	6.42	6.42
Thr 67	$C^{\alpha}H$		3.61		3.83		$C^{\delta}H$	6.60	6.57	6.59	6.61
	$C^{\beta}H$		3.35		3.97	Tyr 151	$C^{\delta}H$		6.19		6.41
	$C^{\gamma 2}H_3$		0.82		1.51		$C^{\epsilon}H$		6.09		6.45
Val 68	$C^{\alpha}H$	2.15	2.19	3.20	3.24	Phe 151	$C^{\delta}H$	6.25		6.49	
	$C^{\beta}H$	0.36	0.40	0.84	0.84		$C^{\epsilon}H$	6.73		6.88	
	$C^{\gamma 1}H_3$	−1.05	−0.93	−0.57	−0.55		$C^{\zeta}H$	6.38		6.56	
	$C^{\gamma 2}H_3$	−3.64	−3.67	−2.32	−2.30						

[a] Chemical shifts in parts per million with respect to residual $^1H^2HO$ at 4.76 ppm, determined at pH* 5.7, 298 K. MbCO values are included for comparison. [b] The denomination 1 and 2 for valines and leucines was attributed according to the NOE data presented in Table III. For histidines, the distinction between C^{δ} and C^{ϵ} protons is based on chemical shift values and is in accordance with the data in Table III. For tyrosines, the distinction between C^{δ} and C^{ϵ} protons is based on strong and unique NOE from the C^{δ} protons to a $C^{\alpha}H$. [c] Determined at pH* 5.7, 298 K (this work); nd, not determined. [d] Taken from Dalvit and Wright (1987); determined at pH* 5.6, 309 K; na, not available. [e] Calculated values reported by Emerson and La Mar (1990).

centered around 7.1 ppm. Identical connectivities are recorded for the sperm whale protein. Figure 4 presents the aromatic region of the DQF-COSY (Figure 4A) and NOESY (Figure 4B) spectra of sperm whale des-Fe Mb. The aromatic protons in contact with Leu 89 belong to a poorly resolved phenylalanine spin system that has NOEs to the 2-vinyl β protons. This assigns it as Phe 138 on the basis of MbCO data and the solid-state structure. Aside from Phe 138, the 2-vinyl protons also have NOEs to a leucine side chain in contact with the α-*meso*-H and the 3-CH_3 group. The $C^{\alpha}H$ and one of the $C^{\delta}H_3$ groups of this leucine are pointing directly toward PrIX, a characteristic of Leu 104.

The β-*meso*-H has strong connectivities to an upfield-shifted aliphatic residue with broad resonances (one of the corresponding cross peaks in horse des-Fe Mb is indicated in Figure 3A, at $\delta_2 = -0.62$ ppm). By using TOCSY spectra, it is possible to trace the side chain completely; it is an isoleucine that has NOEs to the 3-CH_3 group, the 4-vinyl α proton, and Leu 104. In accordance with the X-ray data and sperm whale MbCN NOEs (Ramaprasad et al., 1984), it is assigned as Ile

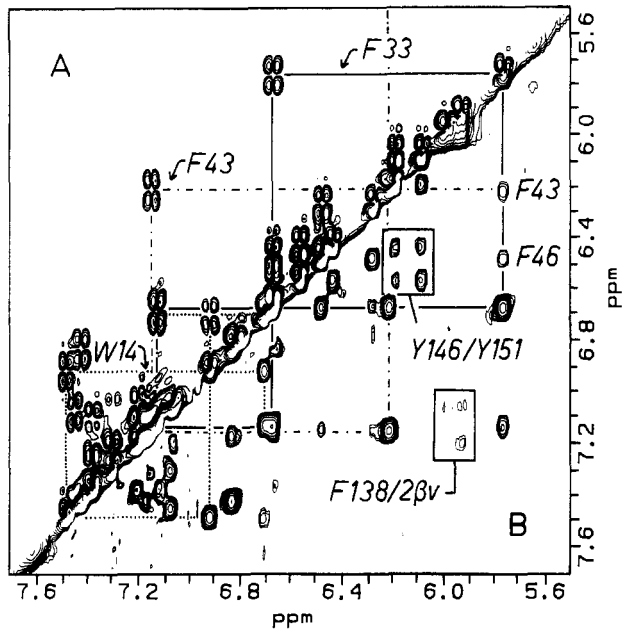

FIGURE 4: Combined DQF-COSY–NOESY spectra of a sample of sperm whale des-Fe Mb in ^2H_2O at pH* 5.7 and 298 K. (A) The DQF-COSY spectrum allows for the identification of several aromatic spin systems. Patterns are indicated for Phe 33 (—), Phe 43 (---, the cross peak at δ_2 = 5.09 ppm is not included), and Trp 14 (···). (B) Corresponding region of the phase-sensitive NOESY spectrum (τ_m = 80 ms). Note the NOEs of Phe 33 to Phe 43 and Phe 46. Phe 138 is identified through its weak NOEs to the 2-β vinyl signals (boxed). A set of NOEs between Tyr 151 and Tyr 146 is also framed.

99. Finally, an NOE from a broad single proton at 8.67 ppm to the γ-*meso*-H leads to the C$^\epsilon$H proton of His 97 (Figure 2). NOEs to the 6-propionate side chain protons at 4.34 and 3.71 ppm support the assignment.

Phe 33, Phe 46, His 48, and Met 55. In Figure 4B, it is noted that Phe 43 has several NOEs to two other phenylalanine rings. This network of connectivities, which is observed in sperm whale MbCO (Dalvit & Wright, 1987) and MbCN (Emerson et al., 1988), is known to arise from Phe 33 and Phe 46. The two phenylalanines can be distinguished by their direct neighbors: Phe 33 is near Met 55 and Phe 46 is near His 48. In des-Fe Mb, the phenylalanine with chemical shifts closest to those of MbCO Phe 46 is in dipolar contact with a histidine ring, consequently assigned as His 48. The δ protons of Phe 46 have a strong NOE to a C$^\alpha$H resonating at ca. 5.1 ppm and attributed to the same residue. The NOE from this proton to the C$^\epsilon$H of His 48 is clearly detected, in agreement with the solid-state prediction. The NOE data contained in Figure 5 establish the proximity of aromatic rings to protons resonating in the 2.35–1.55 ppm region of the spectrum. They demonstrate that the phenylalanine pattern most resembling Phe 33 has an NOE to the sharp singlet of a methionine methyl group at 1.71 ppm (cross peak a). The latter is therefore assigned as Met 55.

Leu 29 and His 64. Correlated experiments identify a leucine residue with methyl groups at −0.15 and −0.48 ppm (Figure 3A). In agreement with NMR data on MbCO, weak NOEs to the Val 68 C$^{\gamma 1}$H$_3$ at ca. −1 ppm and to the rings of Phe 43 and Phe 46 as well as stronger effects to Phe 33 assign Leu 29. The methyl groups of Leu 29 exhibit NOE cross peaks to a broad signal at ca. 4.95 ppm in both horse and sperm whale des-Fe Mb. These are shown in Figure 6, panels B and C. The 4.95 ppm signal arises from a proton in dipolar contact with three residues close to the prosthetic group, Val 68 (Figure 6, upper panels), Phe 43, and Phe 46 (weaker connectivities). The central position points to the distal histidine (His 64). An analogous pattern of NOEs to residues 29 and 68 (Figure 6A), 43, and 46 is observed from His 64 C$^\delta$H in MbCO, which suggests assignment to this proton.

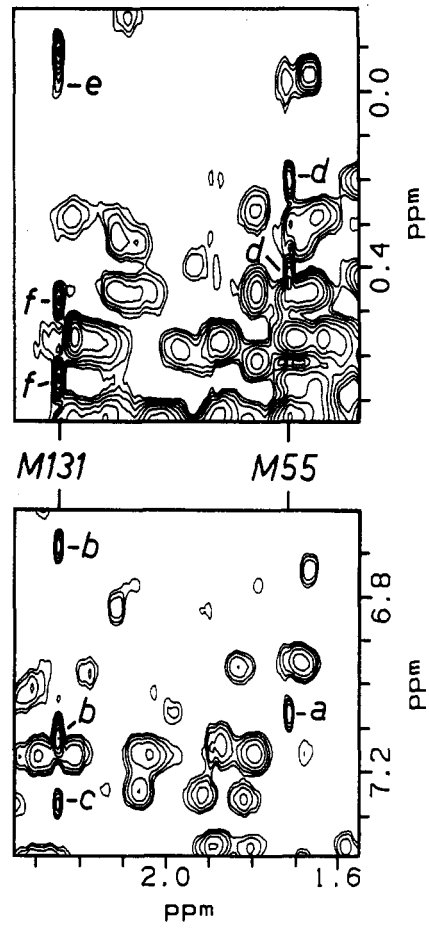

FIGURE 5: Region of a phase-sensitive NOESY spectrum illustrating selected connectivities of the two Met C$^\epsilon$H$_3$ groups in horse des-Fe Mb (conditions as in Figure 1). Cross peaks are labeled as follows: a, Met 55 to Phe 33; b, Met 131 to Trp 14; c, Met 131 to Phe 123; d, Met 55 to Leu 40; e, Met 131 to Val 17; f, Met 131 to Leu 115.

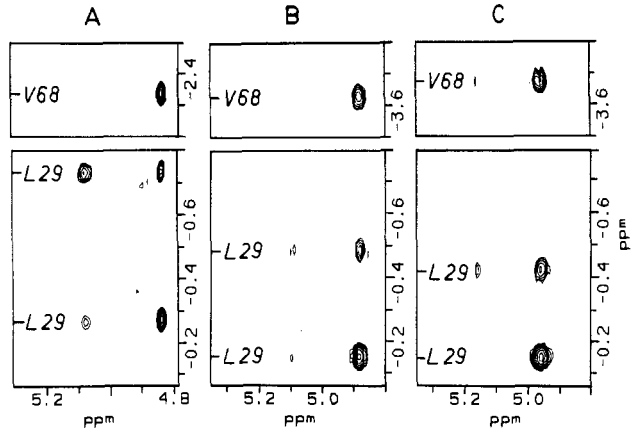

FIGURE 6: Regions of phase-sensitive NOESY spectra with characteristic His 64 connectivities. All spectra recorded in ^2H_2O at pH* 5.7 and 298 K. (A) Horse MbCO (τ_m = 150 ms). (B) Horse des-Fe Mb (τ_m = 160 ms). (C) Sperm whale des-Fe Mb (τ_m = 80 ms). The lower panels show the NOEs between Leu 29 C$^{\delta 1}$H$_3$ and C$^{\delta 2}$H$_3$ and His 64 C$^\delta$H at 4.83 ppm (A), 4.96 ppm (B), and 4.95 ppm (C). The upper panels contain a cross peak connecting the tentative His 64 C$^\delta$H to the C$^{\gamma 2}$H$_3$ of Val 68. Note the chemical shift offset for these sections.

His 36, Ala 94, Phe 106, Ile 142, Tyr 146, and Tyr (Phe) 151. Horse des-Fe Mb possesses two tyrosine side chains, at positions 103 and 146, only one of which gives rise to a typical

Table III: NOE Connectivities Observed in Horse and Sperm Whale Des-Iron Myoglobin[a]

residue	proton(s)[b]	to residue and proton(s)[b]	residue	proton(s)[b]	to residue and proton(s)[b]
Leu 2	$C^{\delta 1}H_3$	W7C^{δ}H, W7N^{ϵ}H, W7$C^{\zeta 2}$H, W7C^{η}H	Val 68	$C^{\gamma 1}H_3$	*α-meso*-H, *δ-meso*-H, 1-CH_3, 2-vinyl *β*-H, L69$C^{\delta 2}H_3$
	$C^{\delta 2}H_3$	W7C^{δ}H, W7N^{ϵ}H, W7$C^{\zeta 2}$H, W7C^{η}H, W7$C^{\zeta 3}$H, W7$C^{\epsilon 3}$H		$C^{\gamma 2}H_3$	*δ-meso*-H, 1-CH_3, 8-CH_3, L29$C^{\delta 1}H_3$, L29$C^{\delta 2}H_3$, H64C^{δ}H, V/T67$C^{\gamma 1/2}H_3$
Trp 7	C^{δ}H	L2$C^{\delta 1}H_3$, L2$C^{\delta 2}H_3$	Leu 69	$C^{\delta 1}H_3$	W14$C^{\zeta 2}$H, W14C^{η}H
	N^{ϵ}H	L2$C^{\delta 1}H_3$, L2$C^{\delta 2}H_3$		$C^{\delta 2}H_3$	W14$C^{\zeta 2}$H, W14C^{η}H, V68$C^{\gamma 1}H_3$
	$C^{\zeta 2}$H	L2$C^{\delta 1}H_3$, L2$C^{\delta 2}H_3$	Ala 71	$C^{\beta}H_3$	*δ-meso*-H, 1-CH_3, 8-CH_3, L89$C^{\delta 1}H_3$
	C^{η}H	L2$C^{\delta 1}H_3$, L2$C^{\delta 2}H_3$	Leu 89	$C^{\delta 1}H_3$	*δ-meso*-H, 1-CH_3, 8-CH_3, A71$C^{\beta}H_3$
	$C^{\zeta 3}$H	L2$C^{\delta 2}H_3$		$C^{\delta 2}H_3$	*δ-meso*-H, 1-CH_3, F138C^{ϵ}H
	$C^{\epsilon 3}$H	L2$C^{\delta 2}H_3$	Ala 94	C^{β}H	Y146C^{δ}H, Y146C^{ϵ}H, F/Y151C^{δ}H
Trp 14	C^{δ}H	V17$C^{\gamma 1}H_3$	His 97	C^{ϵ}H	*γ-meso*-H, 6-propionate *α*-H
	$C^{\zeta 2}$H	V17$C^{\gamma 1}H_3$, L69$C^{\delta 1}H_3$, L69$C^{\delta 2}H_3$	Ile 99	$C^{\gamma 1'}$H	*β-meso*-H, 4-vinyl *α*-H, 5-CH_3
	C^{η}H	V17$C^{\gamma 1}H_3$, L69$C^{\delta 1}H_3$, L69$C^{\delta 2}H_3$		$C^{\gamma 2}H_3$	4-vinyl *α*-H, 3-CH_3, L104$C^{\delta 2}H_3$
	$C^{\zeta 3}$H	V17$C^{\gamma 1}H_3$, V17$C^{\gamma 2}H_3$, L115$C^{\delta 2}H_3$, M131$C^{\epsilon}H_3$	Tyr 103	$C^{\delta,\epsilon}$H	4-vinyl β_{cis}-H
	$C^{\epsilon 3}$H	V17$C^{\gamma 1}H_3$, V17$C^{\gamma 2}H_3$, M131$C^{\epsilon}H_3$	Leu 104	C^{α}H	*α-meso*-H, 3-CH_3
Val 17	$C^{\gamma 1}H_3$	W14C^{δ}H, W14$C^{\zeta 2}$H, W14C^{η}H, W14$C^{\zeta 3}$H, W14$C^{\epsilon 3}$H, H24C^{δ}H, H24C^{ϵ}H		$C^{\delta 1}H_3$	I142$C^{\gamma 2}H_3$, I142$C^{\delta}H_3$
	$C^{\gamma 2}H_3$	W14$C^{\zeta 3}$H, W14$C^{\epsilon 3}$H, H24C^{δ}H, H24C^{ϵ}H, L115$C^{\delta 1}H_3$, L115$C^{\delta 2}H_3$, H119C^{δ}H, M131$C^{\epsilon}H_3$		$C^{\delta 2}H_3$	*α-meso*-H, I99$C^{\gamma 2}H_3$
His 24	C^{δ}H	V17$C^{\gamma 1}H_3$, V17$C^{\gamma 2}H_3$, L115$C^{\delta 1}H_3$, L115$C^{\delta 2}H_3$, H119C^{δ}H	Phe 106	C^{δ}H	H36C^{δ}H, H36C^{ϵ}H
				$C^{\epsilon/\zeta}$H	H36C^{δ}H, H36C^{ϵ}H
	C^{ϵ}H	V17$C^{\gamma 1}H_3$, V17$C^{\gamma 2}H_3$, H119C^{δ}H, H119C^{ϵ}H	Leu 115	$C^{\delta 1}H_3$	V17$C^{\gamma 2}H_3$, H24C^{δ}H, H119C^{δ}H, F123C^{ϵ}H, M131$C^{\epsilon}H_3$
Leu 29	$C^{\delta 1}H_3$	F33C^{ζ}H, H64C^{δ}H, V68$C^{\gamma 2}H_3$		$C^{\delta 2}H_3$	W14$C^{\zeta 3}$H, V17$C^{\gamma 2}H_3$, H24C^{δ}H, H119C^{δ}H, M131$C^{\epsilon}H_3$
	$C^{\delta 2}H_3$	F33C^{ϵ}H, F33C^{ζ}H, H64C^{δ}H, V68$C^{\gamma 2}H_3$			
Phe 33	C^{δ}H	L40$C^{\delta 1}H_3$, L40$C^{\delta 2}H_3$, M55$C^{\epsilon}H_3$	His 119	C^{δ}H	V17$C^{\gamma 2}H_3$, H24C^{δ}H, H24C^{ϵ}H, L115$C^{\delta 1}H_3$, L115$C^{\delta 2}H_3$
	C^{ϵ}H	L29$C^{\delta 2}H_3$, L40$C^{\delta 1}H_3$, L40$C^{\delta 2}H_3$, F43C^{ϵ}H, M55$C^{\epsilon}H_3$		C^{ϵ}H	H24C^{ϵ}H
	C^{ζ}H	L29$C^{\delta 1}H_3$, L29$C^{\delta 2}H_3$, F43C^{δ}H, F43C^{ϵ}H, F43C^{ζ}H, F46C^{δ}H, F46C^{ϵ}H	Phe 123	C^{ϵ}H	L115$C^{\delta 1}H_3$, M131$C^{\epsilon}H_3$
			Met 131	$C^{\epsilon}H_3$	W14$C^{\zeta 3}$H, W14$C^{\epsilon 3}$H, V17$C^{\gamma 2}H_3$, L115$C^{\delta 1}H_3$, L115$C^{\delta 2}H_3$, F123C^{ϵ}H
His 36	C^{δ}H	F106C^{δ}H, F106$C^{\epsilon/\zeta}$H			
	C^{ϵ}H	F106C^{δ}H, F106$C^{\epsilon/\zeta}$H	Phe 138	C^{δ}H	I142$C^{\delta}H_3$
Leu 40	$C^{\delta 1}H_3$	F33C^{δ}H, F33C^{ϵ}H, M55$C^{\epsilon}H_3$		C^{ϵ}H	2-vinyl *α*-H, 2-vinyl *β*-H, L89$C^{\delta 2}H_3$, I142$C^{\delta}H_3$
	$C^{\delta 2}H_3$	F33C^{δ}H, F33C^{ϵ}H, M55$C^{\epsilon}H_3$			
Phe 43	C^{δ}H	*β-meso*-H, F33C^{ζ}H, F46C^{δ}H, F46C^{ϵ}H, F46C^{ζ}H		C^{ζ}H	2-vinyl *α*-H, 2-vinyl *β*-H, I142$C^{\delta}H_3$
	C^{ϵ}H	*β-meso*-H,5-CH_3, F33C^{ϵ}H, F33C^{ζ}H, H64C^{δ}H	Ile 142	$C^{\gamma 2}H_3$	L104$C^{\delta 1}H_3$, Y146C^{δ}H, Y146C^{ϵ}H
	C^{ζ}H	*β-meso*-H, F33C^{ζ}H, H64C^{δ}H		$C^{\delta}H_3$	L104$C^{\delta 1}H_3$, F138C^{δ}H, F138C^{ϵ}H, F138C^{ζ}H, Y146C^{ϵ}H
Phe 46	C^{α}H	F46C^{δ}H, H48C^{ϵ}H			
	C^{δ}H	F33C^{ζ}H, F43C^{δ}H, F46C^{α}H, H48C^{ϵ}H	Tyr 146	C^{δ}H	A94$C^{\beta}H_3$, I142$C^{\gamma 2}H_3$, F/Y151C^{δ}H, F/Y151C^{ϵ}H
	C^{ϵ}H	F33C^{ζ}H, F43C^{δ}H, H64C^{δ}H		C^{ϵ}H	A94$C^{\beta}H_3$, I142$C^{\gamma 2}H_3$, I142$C^{\delta}H_3$, F/Y151C^{δ}H, F/Y151C^{ϵ}H
	C^{ζ}H	F43C^{δ}H			
His 48	C^{ϵ}H	F46C^{α}H, F46C^{β}H	Phe/Tyr 151	C^{δ}H	A94$C^{\beta}H_3$, Y146C^{δ}H, Y146C^{ϵ}H
Met 55	$C^{\epsilon}H_3$	F33C^{δ}H, F33C^{ϵ}H, L40$C^{\delta 1}H_3$, L40$C^{\delta 2}H_3$		C^{ϵ}H	Y146C^{δ}H, Y146C^{ϵ}H
His 64	C^{δ}H	L29$C^{\delta 1}H_3$, L29$C^{\delta 2}H_3$, F43C^{ϵ}H, F43C^{ζ}H, F46C^{ϵ}H, V68$C^{\gamma 2}H_3$			
Val/Thr 67	$C^{\gamma 1/2}H_3$	*γ-meso*-H, *δ-meso*-H, 8-CH_3, V68$C^{\gamma 2}H_3$			

[a] NOEs were determined at pH* 5.7, 298 K, with a mixing time of 80 ms. Only the effects essential to assignment and geometry are listed. Residues at variance between the two proteins are listed as horse/sperm whale. [b] The denomination 1 and 2 for methyl groups of valines and leucines is chosen according to solid-state structure predictions (Hanson & Schoenborn, 1981).

DQF-COSY pattern at 6.44 and 6.60 ppm. The C^{δ} (or C^{ϵ}) protons of Tyr 103 are detected at 7.18 ppm in the spectrum of horse des-Fe Mb through a weak NOE to the 4-vinyl β_{cis}-H. Scalar connectivity to the other ring protons could not be found unambiguously, probably because the cross peaks arise in the 7.20–7.40 ppm region of the spectrum, which is crowded with many aromatic resonances. The Tyr 103 protons resonating at 7.18 ppm are near a phenylalanine residue with overlapping C^{ϵ} and C^{ζ} protons, identified as such via 2Q spectra. This phenylalanine ring, in turn, has strong NOEs in the 8.4–7.8 ppm region of the spectrum, which are illustrated in Figure 7B along with corresponding data on MbCO (Figure 7A). Cross peaks b and c manifest the proximity of a histidine C^{ϵ}H. By analogy to sperm whale MbCO, the pair is assigned as Phe 106 and His 36.

Tyr 146 is the better resolved of the two tyrosines. With Phe 138, it yields NOEs to a resolved isoleucine spin system (some relevant *J* cross peaks are indicated in Figure 3A), which is consequently assigned to Ile 142. Position 151, where a third tyrosine is found in the sperm whale protein, is occupied by a phenylalanine. Because Phe 151 is the only aromatic replacement, it can be identified as the phenylalanine spin system unique to the horse spectrum. It yields a well-resolved and relatively sharp set of peaks at 6.26, 6.38, and 6.73 ppm. Phe 151 and Tyr 146 are in close proximity and have NOEs in common, including strong effects to a group at 0.77 ppm. The corresponding correlated data are characteristic of an alanine $C^{\beta}H_3$ and this leads to the assignment of Ala 94, a residue that exhibits the same NOE network in MbCO.

In sperm whale des-Fe Mb, Tyr 146 is readily recognized by its DQF-COSY cross peaks at the same chemical shift as in the horse protein (Figure 4A). Tyr 146 presents strong ring-to-ring NOEs to a tyrosine residue at 6.18 and 6.09 ppm (Figure 4B) absent from the horse des-Fe Mb spectrum. This points to Tyr 151. Figure 8 is a section of the phase-sensitive NOESY spectrum introduced in Figure 4B containing cross peaks between the aromatic rings and upfield-shifted aliphatic protons. Among them are labeled those of Tyr 146 and Tyr 151 to an alanine residue, Ala 94, and those of Tyr 146 and Phe 138 to a resolved isoleucine spin system, Ile 142. Unambiguous assignment of Tyr 103 was not possible under our experimental conditions.

Trp 14, Val 17, His 24, Leu 69, Leu 115, His 119, Phe 123, and Met 131. Trp 14 and Trp 7 are located farther away from the binding site. In this region of the protein, the better match of chemical shifts between des-Fe Mb and MbCO simplifies the task of analyzing the spectrum. The signals from the rings of Trp 7 and Trp 14 are readily recognized through DQF-

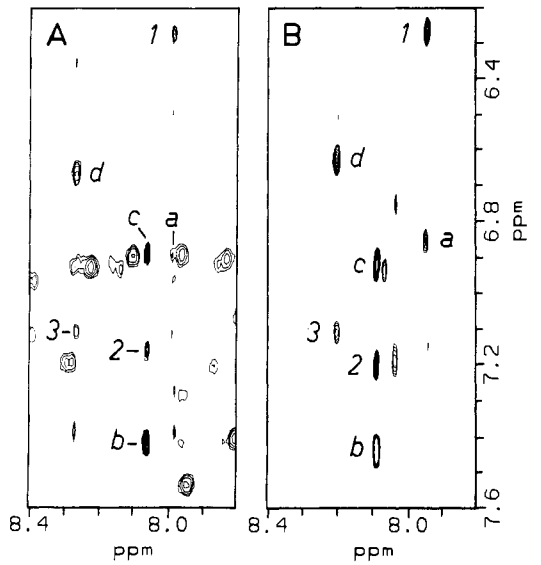

FIGURE 7: Region of phase-sensitive NOESY spectra of horse Mb recorded in ^2H_2O and at 298 K showing the connectivities involving His residues 24, 36, 48, and 119. (A) MbCO, pH* 5.7, τ_m = 150 ms. (B) Des-Fe Mb, pH* 5.7, τ_m = 160 ms. For clarity, the cross peaks are numbered: 1, His 24 $C^\delta H/C^\epsilon H$; 2, His 36 $C^\delta H/C^\epsilon H$; 3, His 48 $C^\delta H/C^\epsilon H$; a, His 24 $C^\epsilon H$ to His 119 $C^\delta H$; b, His 36 $C^\epsilon H$ to Phe 106 $C^\epsilon H$, $C^\zeta H$; c, His 36 $C^\epsilon H$ to Phe 106 $C^\delta H$; d, His 48 $C^\epsilon H$ to Phe 46 $C^\delta H$. Additional peaks in (A) arise from incompletely exchanged amide protons.

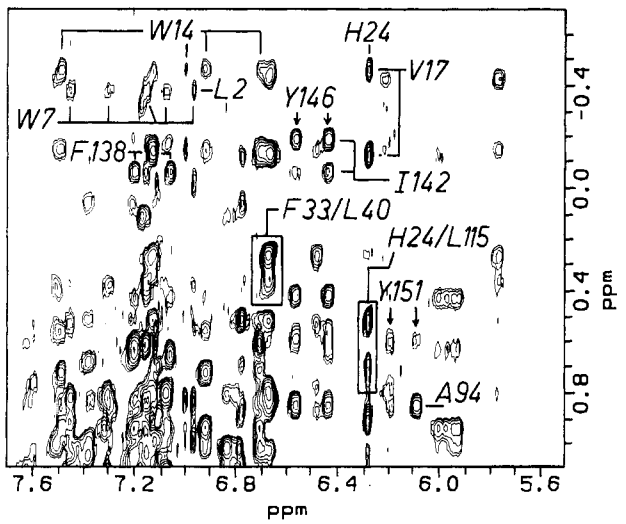

FIGURE 8: Region of the phase-sensitive NOESY spectrum (τ_m = 80 ms) of sperm whale Mb, recorded in ^2H_2O at pH* 5.7 and 298 K. The δ_2 range matches that in Figure 4, while the δ_1 range corresponds to upfield-shifted aliphatic resonances. The connectivities discussed in the text are marked.

COSY, 2Q, and TOCSY experiments. The NOESY data of Figure 2 contain part of these two spin systems; both N^ϵ protons are seen in contact with their respective $C^\delta H$ and $C^{\zeta 2}H$. Trp 14 is expected to display NOEs to the $C^\epsilon H_3$ of Met 131. Figure 5 shows a relevant portion of the NOESY spectrum where one of the tryptophan rings has strong dipolar connectivities to a sharp, non-porphyrin methyl group at 2.25 ppm. Since Met 55 $C^\epsilon H_3$ was assigned at 1.71 ppm, these NOEs must arise from Met 131. Met 131 leads to the aromatic ring of Phe 123: the two side chains are in dipolar contact (Figure 5, cross peak c), as observed in MbCO.

Other NOEs to Trp 14 include those from a shifted valine residue (Figure 8). The methyl groups of this valine are also in contact with a histidine ring at 6.28 and 7.85 ppm. As in MbCO, assignment follows to Val 17 and His 24. Inspection of the solid-state structure reveals close proximity of the side chains of Trp 14, Val 17, and His 24 to that of Leu 115. A residue with geminal methyl groups at 0.51 and 0.68 ppm presents strong NOEs to the required residues. This provides a tentative assignment for Leu 115. Also in contact with His 24 is another histidine, which is recognized as His 119 by analogy to MbCO (Figure 7). NOEs between His 119 and Leu 115 reinforce the latter assignment. Trp 14 and Val 68 are both near a residue containing an isopropyl group and implicate the intervening Leu 69.

Trp 7 and Leu 2. The remaining tryptophan side chain is Trp 7 by default. All protons of this ring have NOEs to one methyl group belonging to an upfield-shifted leucine residue (Figure 8). Leu 2, which is located directly above Trp 7 and therefore subject to ring current effects, is the best candidate for this side chain. The other methyl group is in contact with only two ring protons, as predicted by the solid-state structure.

Discussion

The results of the NMR experiments confirm that the main structural features of native Mb are restored by the interactions with PrIX, without a requirement for coordination to a central ion. The binding geometry of the porphyrin to apomyoglobin can be specified by using the assigned resonances of PrIX substituents and binding-site residues. Only one set of signals is observed and therefore PrIX assumes a single orientation with respect to the protein matrix. This provides support for the conclusion reached by La Mar et al. (1989) on the basis of porphyrin *meso*-H and Val 68 $C^{\gamma 2}H_3$ signals. The observed prosthetic group–protein NOEs also demonstrate that the sole orientation is that which is thermodynamically favored for the heme in the holoprotein, i.e., with Ile 99 over the *β-meso*-proton.

The chemical shift values listed in Tables I and II show that displacement from the MbCO line positions is limited to PrIX protons and some residues close to the porphyrin ring. The alteration of chemical shifts can be due to two influences: change in the ring current intensity generated by the prosthetic group and change in relative geometry. The chemical shift difference between the porphyrin substituents in the des-Fe complex and the CO complex [$\Delta\delta = \delta$(des-Fe) − δ(CO)] is systematically positive, with an average value of 0.5 ppm for the meso protons and 0.2 ppm for the methyl groups. This suggests that an increase in the ring current of the porphyrin in des-Fe Mb compared to that of the heme in MbCO may be at work. An exception to the trend of increased ring current is observed for the 4-vinyl group, which exhibits unchanged or negative α shift and large β shift. It is likely that this anomaly stems from the displacement of a nearby protein residue.

It has been proposed that the increase in ring current arises from the partial formation of the porphyrin dication, perhaps through hydrogen bonding to the proximal histidine (La Mar et al., 1989). Breslow et al. (1967) carried out optical studies of des-Fe Mb and reported that the spectrum of des-Fe Mb is independent of pH over the range 5.3–11. They pointed out that the nondegeneracy of the porphyrin Q and B bands between 500 and 700 nm is consistent with a neutral species. In the NMR spectrum, no change in the *meso*-H chemical shifts is observed between pH 5.5 and 9.7 (not shown). The optical evidence, the invariant *meso*-H chemical shifts, and the remarkable constancy of binding-site structure favor a neutral porphyrin. Clarification of this aspect of des-Fe Mb is in progress.

In contrast to the porphyrin, the $\Delta\delta$ values for the protein resonances do not organize into any particular pattern. Since

near the porphyrin ring a considerable shift change can be the consequence of a relatively small geometry perturbation, the deviation from a regular trend may be due to small differences in structure whose manifestations are amplified by substitution for a prosthetic group with more intense ring current. Thus, the structural description reached here relies on NOE connectivities. It compares directly to that presented by Dalvit and Wright (1987). Diagrams identical with those of Figures 12 and 17 in their work apply with a few adjustments as detailed below.

(*i*) *Proximal Side.* Two histidine residues are normally located on the proximal side of the heme: His 93 (proximal) and His 97, which forms a salt bridge to the 7-propionate group. For His 97, only the $C^{\epsilon}H$ was found, at a spectral position similar to that in MbCO and with the expected NOE to the γ-*meso*-H. This signal is broad and no potential $C^{\delta}H$ partner could be identified. NOEs from the $C^{\epsilon}H$ are observed to two protons of the 6-propionate side chain. In the absence of heteronuclear data, the distinction between propionate $C^{\alpha}H$ and $C^{\beta}H$ depends upon dipolar contact considerations. The neutron diffraction structure of the holoprotein places one of the four 6-propionate protons (α'-H) closer to the γ-*meso*-H than the others; this proton is tentatively assigned at 4.34 ppm. His 97 would thus be in contact with the 6-propionate α pair. Such interpretation of the NOE pattern, which assumes that the geometry described by the solid-state structure is adequate, is the most economical and is consistent with His 97 maintaining its salt bridge to the 7-propionate group.

In sperm whale and horse MbCO, the nonexchangeable ring protons of His 93 are shifted upfield from the water line between 1 and 2 ppm. The $C^{\epsilon}H$ is readily recognizable by its NOEs to the $C^{\delta}H_3$s of Leu 89. No such connectivity, or any other ascribable to this residue, was seen in the spectra of the des-Fe proteins. It is known that PrIX is an efficient photosensitizer for the oxidation of His residues; in fact, the destruction of His 93 has been reported in des-Fe Mb (Breslow et al., 1967). To verify the integrity of the myoglobin used in the NMR experiments, holoMb was prepared from protein having contained PrIX (see Materials and Methods). The ^1H_2O spectrum of this material in the metcyano form exhibited intact His 64, His 93, and His 97 ring NH signals (Cutnell et al., 1981). The possibility that histidine oxidation occurred during sample preparation and NMR data collection was therefore eliminated. It should be noted that the residues which normally constitute the direct environment of His 93 are found in their MbCO locations. This is true in particular for Leu 89, Ala 94, His 97, Ile 99, Leu 104, and Phe 138, which are depicted in Figure 9. They define a cavity where His 93 could adopt different conformations once the coordination bond is severed. This cavity is known to accommodate a xenon atom without structural distortion (Takano, 1977a).

Weak NOEs are detected from the C^{δ} (or C^{ϵ}) protons of Tyr 103 to the 4-vinyl β_{cis} proton in horse des-Fe Mb. In horse MbCO, however, these effects are better defined and are accompanied by smaller NOEs to the 4-vinyl β_{trans} proton. That the des-Fe Mb 4-vinyl group does not follow the chemical shift trend set by the other PrIX substituents may be due to relocation of, and therefore altered ring current shift from, Tyr 103.

Leu 89 is an interesting residue located at the edge of the hydrophobic cavity mentioned above. It is highly conserved through the globin family (Bashford et al., 1987) and is the only side chain whose orientation in horse metaquo Mb differs significantly from that in sperm whale Mb (Evans & Brayer, 1988). In both forms of horse Mb studied here, as well as in

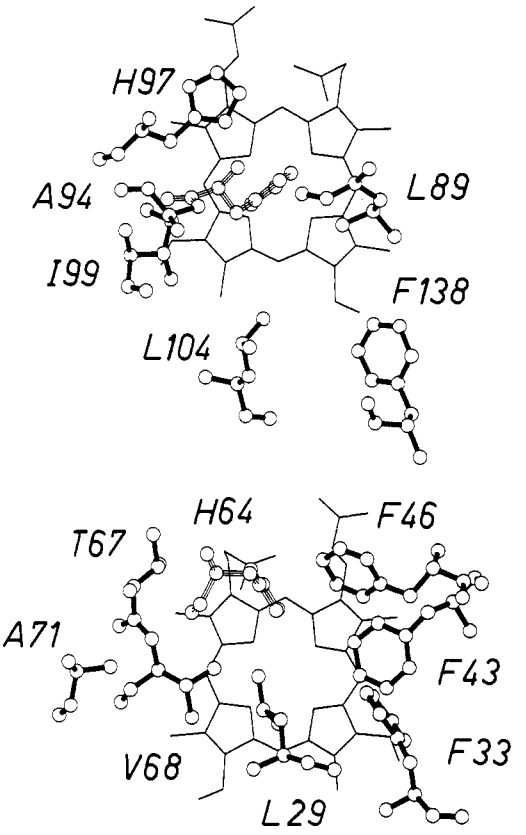

FIGURE 9: The environment of His 93 (upper part) and His 64 (lower part) as described by the X-ray structure of sperm whale MbCO (Kuryian et al., 1986). The viewing axis is perpendicular to the heme plane with the residues of interest above the plane. The residues whose orientation with respect to the porphyrin ring could be determined by NOE spectroscopy are in boldface type. His 93 and His 64 are represented with lighter bonds. Data collected so far place His 64 closer to Leu 29 and Val 68 than represented here.

sperm whale MbCO and des-Fe Mb, its methyl groups yield NOEs to the δ-*meso*-H. NOEs to the 1- and 8-CH_3 groups are also qualitatively preserved, and as a consequence, the side-chain orientation in solution is proposed to be independent of the origin of the protein and the state of coordination of His 93.

The proximal residue Ile 99 was readily assigned in the des-Fe spectrum. Its resonances are broad and most are resolved at chemical shift values upfield from the computed values for MbCO (Emerson & La Mar, 1990). This residue is located as found in the metcyano complex in solution (Ramaprasad et al., 1984) and in the X-ray structures of various liganded forms.

(*ii*) *Distal Side.* The interactions of bulky ligands with distal side residues have been explored by several investigators. Notable examples are isonitriles (Mims et al., 1983; Johnson et al., 1989), phenyl group (Ringe et al., 1984), and trimethylphosphine (Simonneaux et al., 1989). These studies identify the side chains that are most affected by the accommodation of unusually large compounds: Arg 45, His 64, Val 68, and Phe 43 are generally displaced from their physiological positions. Des-Fe Mb can be taken as a representative of the other extreme, illustrating the effect of absence of bound ligand. While the chemical shifts of Phe 43 $C^{\zeta}H$ and all Val 68 protons are perturbed with respect to their MbCO values, no discrepancy with the NOEs predicted by the solid-state structure can be reported at this time. In the case of His 64, only the $C^{\delta}H$ is tentatively assigned, at a spectral position close to that observed in MbCO. It is a broad signal with no scalar connectivity cross peak characteristic of a histidine ring. The

network of NOEs involving it and other assigned residues is consistent with the environment depicted in Figure 9. However, the current NOE intensity data indicate a tilt toward Leu 29 and Val 68 and away from Phe 46 and Phe 43. A more precise geometry determination awaits the assignment of other His 64 signals and the quantitative analysis of NOE build-up experiments. Phe 33, Phe 43, and Phe 46 are freely rotating, as demonstrated by the presence of an average signal for both $C^{\delta}Hs$ and $C^{\epsilon}Hs$.

The integrity of the ligand binding site suggests that des-Fe Mb may mimic deoxymyoglobin, an unstable high-spin complex for which few NMR data are available. Use of the des-Fe complex as a model for the deoxygenated form of an oxygen-binding heme protein has been proposed for hemoglobin (Noble et al., 1972). In the optical spectrum of des-Fe hemoglobin, the peaks corresponding to porphyrin absorption occur at wavelengths similar to those of the porphyrin in neutral aqueous solution. This has led to the proposition that water may be included within the binding site (Sebban et al., 1980). In the case of des-Fe Mb, a more satisfactory analogy is drawn to the porphyrin dissolved in a less polar medium (Breslow et al., 1967). Further experiments are in progress to test the similarity of the des-Fe Mb and deoxy Mb structures.

(*iii*) *Protein Termini.* Several NOEs indicate that the tertiary structure is largely unaffected by iron removal. The dipolar contacts between Met 131 and Trp 14, as well as those between His 24 and His 119, are just two examples. In all the forms studied, His 24 does not appear to be protonated at pH 5.7. The $C^{\delta}H$ signal is insensitive to pH variations above this value, while the $C^{\epsilon}H$ moves moderately, probably reflecting the titration of the nearby His 119. All these observations are consistent with the presence of a hydrogen bond between the two residues (Dalvit & Wright, 1987).

At the C-terminus, residues 146 and 151 adopt the same relative orientation in the three proteins studied here, with the ring of Phe (or Tyr) 151 close enough to the ring of Tyr 146 to yield strong NOEs. NOEs to Ala 94 confirm that the residue at position 151 is in contact with the F helix. In sperm whale MbCO, the ring resonances of 146 and 151 overlap and make the direct observation of 146 $\leftrightarrow$ 151 NOEs difficult. However, the reported NOEs between Tyr 151 and Ala 94 demonstrate that the orientation is also similar. According to the neutron diffraction structure of sperm whale MbCO, all ring protons of Tyr 151 and Tyr 146 are far apart, Tyr 151 pointing toward the solvent and Tyr 146 being locked in place by a hydrogen bond to Ile 99. It appears then that Tyr 151 reorients to dock against the F helix. This is not surprising as the *B* factors for this residue are large and displacement of Tyr 151 has been observed in sperm whale oxymyoglobin (Phillips, 1980). The position of Phe 151 is in agreement with the X-ray structure of horse metaquo Mb (Evans & Brayer, 1988).

Conclusions

The NOEs observed in des-Fe Mb point to a restored holoprotein structure. The fact that the porphyrin binds at the same site as the heme and maintains qualitatively the same contacts with the residues lining the cavity demonstrates that the positioning of the porphyrin is dictated solely by hydrophobic and electrostatic interactions. It appears that the absence of ligand has no major effect on the distal side of the prosthetic group and that on the proximal side the environment of His 93 is largely intact. Structural similarity to the holoprotein extends to the C- and N-termini, where the correct tertiary interactions are detected. However, it remains to investigate which of those features we described existed prior to prosthetic group insertion. In the next paper, we present preliminary data on apoMb that address the question (Cocco & Lecomte, 1990).

Acknowledgments

We thank Drs. C. R. Matthews, T. C. Pochapsky, and C. Royer for useful discussions.

Registry No. *b* heme, 14875-96-8; His, 71-00-1.

References

Albani, J., & Alpert, B. (1986) *Chem. Phys. Lett. 131*, 147–152.

Atassi, M. Z. (1967) *Biochem. J. 103*, 29–35.

Bashford, D., Chothia, C., & Lesk, A. M. (1987) *J. Mol. Biol. 196*, 199–216.

Bax, A., & Davis, D. G. (1985) *J. Magn. Reson. 65*, 355–360.

Bodenhausen, G., Kogler, H., & Ernst, R. R. (1984) *J. Magn. Reson. 58*, 370–388.

Braunschweiler, L., & Ernst, R. R. (1983) *J. Magn. Reson. 53*, 521–528.

Braunschweiler, L., Bodenhausen, G., & Ernst, R. R. (1983) *Mol. Phys. 48*, 535–560.

Braunstein, D., Ansari, A., Berendzen, J., Cowen, B. R., Egeberg, K. D., Frauenfelder, H., Hong, M. K., Ormos, P., Sauke, T. B., Scholl, R., Schulte, A., Sligar, S. G., Springer, B. A., Steinbach, P. J., & Young, R. D. (1988) *Proc. Natl. Acad. Sci. U.S.A. 85*, 8497–8501.

Breslow, E., & Koehler, R. (1965) *J. Biol. Chem. 240*, PC2266–PC2268.

Breslow, E., Koehler, R., & Girotti, A. W. (1967) *J. Biol. Chem. 242*, 4149–4156.

Cocco, M. J., & Lecomte, J. T. J. (1990) *Biochemistry* (following paper in this issue).

Cutnell, J. D., La Mar, G. N., & Kong, S. B. (1981) *J. Am. Chem. Soc. 103*, 3567–3572.

Dalvit, C., & Wright, P. E. (1987) *J. Mol. Biol. 194*, 313–327.

Davis, D. G. (1989) *J. Magn. Reson. 81*, 603–607.

Dayhoff, M. O. (1976) *Atlas of Protein Sequence and Structure*, Vol. 5, Suppl. 2, National Biomedical Research Foundation, Washington, DC.

Drobny, G., Pines, A., Sinton, S., Weitekamp, D. P., & Wemmer, D. (1979) *Symp. Faraday Soc. 13*, 49–55.

Emerson, S. D., & La Mar, G. N. (1990) *Biochemistry 29*, 1556–1566.

Emerson, S. D., Lecomte, J. T. J., & La Mar, G. N. (1988) *J. Am. Chem. Soc. 110*, 4176–4182.

Evans, S. V., & Brayer, G. D. (1988) *J. Mol. Biol. 263*, 4263–4268.

Griko, Y. V., Privalov, P. L., Venyaminov, S. Y., & Kutyshenko, V. P. (1988a) *Biofizika 33*, 18–26.

Griko, Y. V., Privalov, P. L., Venyaminov, S. Y., & Kutyshenko, V. P. (1988b) *J. Mol. Biol. 202*, 127–138.

Hanson, J. C., & Schoenborn, B. P. (1981) *J. Mol. Biol. 153*, 117–146.

Harrison, S. C., & Blout, E. R. (1965) *J. Biol. Chem. 240*, 299–303.

Johnson, K. A., Olson, J. S., & Phillips, G. N. (1989) *J. Mol. Biol. 207*, 459–463.

Kumar, A., Ernst, R. R., & Wüthrich, K. (1980) *Biochem. Biophys. Res. Commun. 95*, 1–6.

Kuriyan, J., Wilz, S., Karplus, M., & Petsko, G. A. (1986) *J. Mol. Biol. 192*, 133–154.

La Mar, G. N., Pande, U., Hauksson, J. B., Pandey, R. K., & Smith, K. M. (1989) *J. Am. Chem. Soc. 111*, 485–491.

Mabbutt, B. C., & Wright, P. E. (1985) *Biochim. Biophys. Acta 832*, 175–185.

Marion, D., & Wüthrich, K. (1983) *Biochem. Biophys. Res. Commun. 113*, 967–974.
Mauk, M. R., & Girotti, A. W. (1973) *Biochemistry 12*, 3187–3193.
Mims, M., Olson, J. S., Russu, I. M., Miura, S., Cedel, T. E., & Ho, C. (1983) *J. Biol. Chem. 258*, 6125–6134.
Noble, R. W., Rossi, G. L., & Berni, R. (1972) *J. Mol. Biol. 70*, 689–696.
Otting, G., Widmer, H. Wagner, G., & Wüthrich, K. (1986) *J. Magn. Reson. 66*, 187–193.
Phillips, S. E. V. (1980) *J. Mol. Biol. 142*, 531–554.
Ramaprasad, S., Johnson, R. D., & La Mar, G. N. (1984) *J. Am. Chem. Soc. 106*, 5330–5335.
Rance, M., & Wright, P. E. (1986) *J. Magn. Reson. 66*, 372–378.
Rance, M., Sørensen, O. W., Bodenhausen, G., Wagner, G., Ernst, R. R., & Wüthrich, K. (1983) *Biochem. Biophys. Res. Commun. 117*, 479–485.
Ringe, D., Petsko, G. A., Kerr, D. E., & Ortiz de Montellano, P. R. (1984) *Biochemistry 23*, 2–4.
Sebban, P., Copper, M., Alpert, B., Lindqvist, L., & Jameson, D. M. (1980) *Photochem. Photobiol. 32*, 727–731.
Simonneaux, G., Bondon, A., Sodano, P., & Sinbandhit, S. (1989) *Biochim. Biophys. Acta 999*, 42–45.
Springer, B. A., Egeberg, K. D., Sligar, S. G., Rohlfs, R. J., Mathews, A. J., & Olson, J. S. (1989) *J. Biol. Chem. 264*, 3057–3060.
Takano, T. (1977a) *J. Mol. Biol. 110*, 537–568.
Takano, T. (1977b) *J. Mol. Biol. 110*, 569–584.
Teale, F. W. J. (1955) *Biochim. Biophys. Acta 35*, 289.
Varadarajan, R., Zewert, T., Gray, H. B., & Boxer, S. G. (1989a) *Science 243*, 69–72.
Varadarajan, R., Lambright, D. G., & Boxer, S. G. (1989b) *Biochemistry 28*, 3771–3781.

Characterization of Hydrophobic Cores in Apomyoglobin: A Proton NMR Spectroscopy Study†

Melanie J. Cocco and Juliette T. J. Lecomte*

Department of Chemistry, 152 Davey Laboratory, The Pennsylvania State University, University Park, Pennsylvania 16802

Received July 23, 1990; Revised Manuscript Received August 30, 1990

ABSTRACT: A proton nuclear magnetic resonance spectroscopic study of horse apomyoglobin was undertaken in order to define the regions of myoglobin that are and that are not structurally affected by the binding of the prosthetic group. It was found that, in spite of the poor spectral resolution, a number of spin systems could be identified by using standard correlated methods. Four clusters consisting mostly of hydrophobic residues were detected by nuclear Overhauser spectroscopy, two of which involved the tryptophan side chains. Extensive similarities to nuclear Overhauser spectroscopy data collected on the carbonmonoxy form of holomyoglobin suggested tentative assignments for several residues. It appeared that distinct cores of side chains on the distal side of the binding pocket and between the A, B, G, and H helices maintain the same packing as they do in holomyoglobin and apomyoglobin reconstituted with protoporphyrin IX.

Myoglobin is a monomeric heme protein of 17 kDa that in its native state is ca. 70% helical (Takano, 1977a,b; Evans & Brayer, 1988). The regular secondary structure is organized into eight helices, denominated A through H, with the heme contained in a cavity defined mostly by the E and F helices. Apomyoglobin (apoMb),[1] the proteinic component of myoglobin, is known to possess fewer residues in helical conformation than the holoprotein (Harrison & Blout, 1965; Kawamura-Konishi et al., 1988). Various physical techniques have contributed to a fragmentary description of the apoprotein structure. Fluorescence depolarization and lifetime measurements of sperm whale apoMb (Anderson et al., 1970) have shown that the environment of the two tryptophans is practically unchanged on going from the holo- to the apoprotein. These fluorescence results along with folding studies of human apoMb mutated at position 110 (Hughson & Baldwin, 1989) indicate that the A, B, G, and H helices are at least partially formed and dock properly through hydrophobic interactions. The presence of an extensive hydrophobic core is consistent with differential scanning calorimetry experiments reporting the cooperative thermal unfolding of apoMb (Griko et al., 1988).

In the preceding paper (Lecomte & Cocco, 1990), we presented an NMR study of apomyoglobin combined with protoporphyrin IX and confirmed the observation of Breslow et al. (1967) that the hydrophobic and ionic interactions involving the prosthetic group are sufficient to restore the native fold. In order to describe the conformational change triggered by heme (or protoporphyrin IX) insertion within the protein matrix, we initiated the characterization of the apoprotein by the same methods. We show here that limited but valuable information can be obtained on apoMb by standard two-di-

† Acknowledgement is made to the donors of the Petroleum Research Fund, administered by the American Chemical Society, for support of this work.

* To whom correspondence should be addressed.

[1] Abbreviations: apoMb, apomyoglobin; CD, circular dichroism; des-Fe Mb, des-iron myoglobin; COSY, correlated spectroscopy; 2D, two-dimensional; DQF-COSY, double-quantum-filtered COSY; holoMb, holomyoglobin; Mb, myoglobin; MbCO, carbonmonoxymyoglobin; NMR, nuclear magnetic resonance; NOE, nuclear Overhauser effect; NOESY, two-dimensional proton nuclear Overhauser spectroscopy; TOCSY, total correlation spectroscopy; 2Q, two-quantum.

0006-2960/90/0429-11067$02.50/0